Cu_2ZnSnS_4 thin films prepared by sulfurization of co-electrodeposited metallic precursors

M. Valdés, Y. Di Iorio, K. Castañeda, R. E. Marotti & M. Vázquez

Journal of Applied Electrochemistry

ISSN 0021-891X

J Appl Electrochem
DOI 10.1007/s10800-017-1072-3

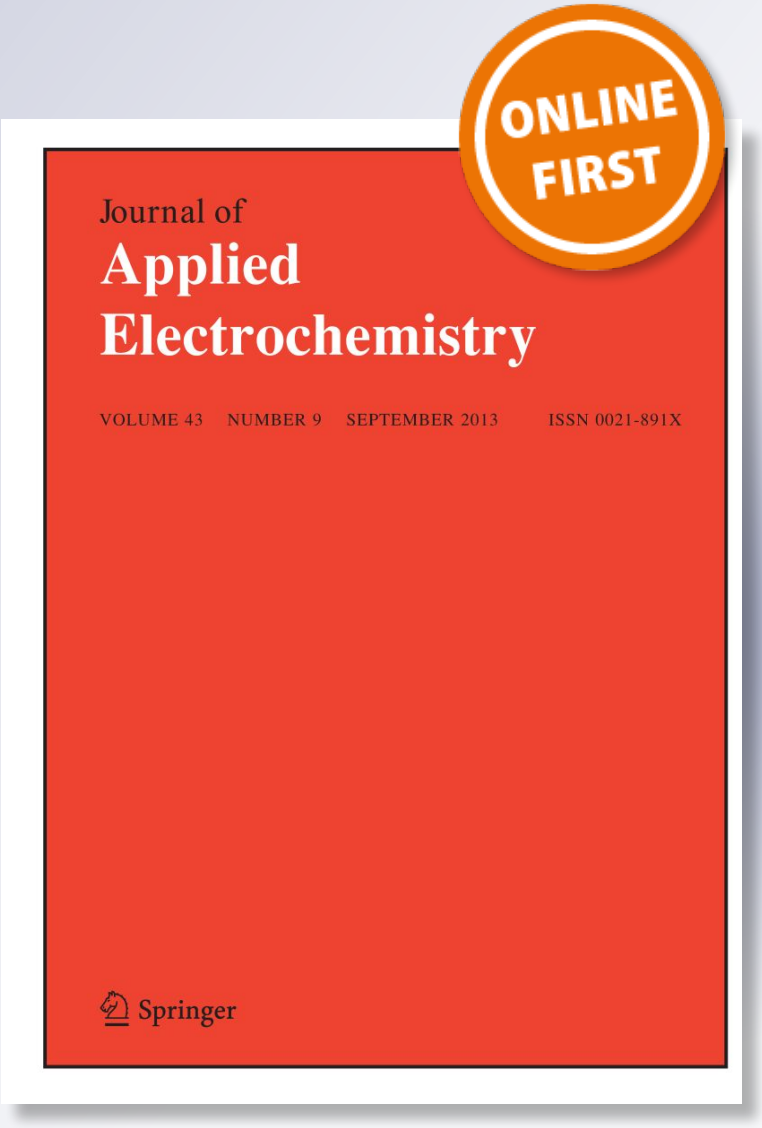

Springer

J Appl Electrochem
DOI 10.1007/s10800-017-1072-3

RESEARCH ARTICLE

Cu_2ZnSnS_4 thin films prepared by sulfurization of co-electrodeposited metallic precursors

M. Valdés[1] · Y. Di Iorio[1] · K. Castañeda[2] · R. E. Marotti[3] · M. Vázquez[1]

Received: 8 December 2016 / Accepted: 21 March 2017

Abstract Cu_2ZnSnS_4 (CZTS) thin films were prepared by thermal sulfurization of co-electrodeposited CuZnSn (CZT) metal precursors. Electrodeposition times between 10 and 40 min were used to study the influence of this parameter on the composition, structure, thickness, and morphology of the sulfurized films. CZT precursors and CZTS films were characterized by X-ray diffraction (XRD), energy-dispersive spectroscopy (EDS), and Raman spectroscopy. The morphologies were evaluated by electronic microscopy. The electrodeposition time was found to influence the chemical composition of the metal precursor, especially the Cu and Sn content. Furthermore, XRD results showed the formation of Cu_5Zn_8, while Sn seemed to be present in an amorphous state. A cauliflower-like morphology was observed in the precursors, especially at long deposition times, which can be related to an electrodeposition mechanism controlled by mass transfer. A significant increase of the film thickness was observed after sulfurization. The morphology changed to round particles and presented a bi-layered structure with an internal compact layer of nanometer size particles and an external layer formed by micrometer-size particles. Raman spectroscopy, XRD, and EDS measurements confirmed the formation of crystalline CZTS after sulfurization. In addition, a disperse Cu_2S secondary phase co-existed in the film. Increasing the precursor deposition time increased the amount of secondary phases in the film after sulfurization. Direct energy gap values close to 1.5 eV were estimated for CZTS films using transmittance spectra in the infrared region. CZTS films obtained with short electrodeposition times are promising as absorbers in kesterite thin films solar cells.

Graphical Abstract

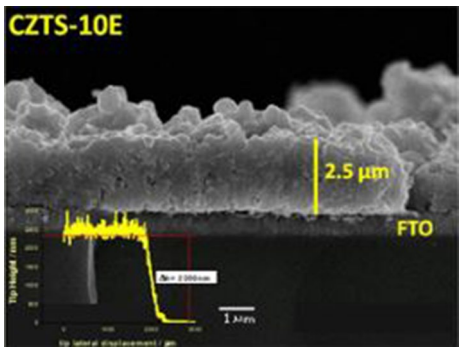

Keywords Co-electrodeposition · Sulfurization · Cu_2ZnSnS_4 · Kesterite

1 Introduction

Cu_2ZnSnS_4 (CZTS) is a quaternary semiconductor that has emerged as a potential absorber substitute for $CuInGaSe_2$ in photovoltaic devices. This material has excellent optical properties ($\alpha \geq 10^5$ cm^{-1}) and a direct bandgap energy value (E_{GAP}) that matches the solar spectrum (1.4 eV $\leq E_{GAP} \leq$ 1.5 eV) [1, 2]. Furthermore, it does not

✉ M. Vázquez
mvazquez@fi.mdp.edu.ar

[1] Electroquímica Aplicada, INTEMA, Facultad de Ingeniería, CONICET-Universidad Nacional de Mar del Plata, Juan B. Justo 4302 B7608FDQ Mar del Plata, Argentina

[2] Grupo de Física de Materiales Orgánicos e Inorgánicos, Universidad del Quindío, Carrera 15 Calle 12 Norte, Armenia, Quindío, Colombia

[3] Instituto de Física, Facultad de Ingeniería, Universidad de la República, Julio Herrera y Reissig 565, C.C. 30 11000 Montevideo, Uruguay

Published online: 25 March 2017

contain toxic elements such as selenium or expensive and scarce ones as indium and gallium. Due to these properties, CZTS films are being intensively studied and are excellent candidates for developing low-cost, highly efficient, and environmentally friendly solar cells [3–7].

In order to achieve real cost reductions, the deposition of thin films should involve inexpensive equipment and be easily transferable to industrial scale. Electrodeposition meets all these requirements and has been used for decades in coatings with applications in several fields [8].

Different electroplating routes to obtain CZTS have been reported. Recently Colombara et al. have published a review giving detailed information of the main electrodeposition routes for CZTS [9]. In general, three main methodologies have been employed so far. The most commonly used one involves the electroplating of stacked layers of individual elements, followed by a treatment in sulfur atmosphere to transform the precursor into CZTS [10, 11]. This approach, called the stacked elemental layers route (SEL), has led to high-quality kesterite films yielding efficiencies of 8.2% for a pure-selenide $CuZnSnSe_4$ (CZTSe) device [12] and 8% for a pure-sulfide CZTS device [13]. A second method employs one-step electrodeposition of all constituents adding a sulfur source into the electrolyte [14–16]. In our previous work [17], we used this method and found some problems related to the stability of the sulfur source in the precursor, causing delamination of the films at electrodeposition potentials higher than −0.85 V (vs. SCE). Moreover, real sulfur incorporation in the material was achieved after the sulfurization stage. A third route requires the preparation of a Cu–Zn–Sn precursor (CZT) in the so-called co-electrodeposition approach, to later incorporate S by sulfurization during annealing and so transform the precursor into CZTS [18–24]. In the last couple of years, this route has attracted particular attention. Cheng et al. [25] explored the electrodeposition on FTO by adjusting the pH value of the electrolytic solution to 7.0 using diethanol amine and using two potentials and two annealing temperatures. They achieved the deposition of high-quality CZTS films fabricated from CZT precursors applying a deposition potential of −1.3 V (vs. Ag/AgCl) during 20 min and 580 °C as sulfurization temperature. Li et al. [23] investigated the influence of two different sulfurization processes on the morphological and structural properties of CZTS prepared on Mo-coated glass. They found that a close-zone annealing in S vapor leads to the formation of CZTS absorbers with large grains and less additional phases. Hreid et al. [26] explored the effect of different concentrations of Cu(II), Zn(II), and Sn(II) ions in the electrolytic bath solution on the properties of electrochemically deposited CZT. They found that the metal content in the CZT films was linearly dependent on the concentration of the corresponding metal ion in the precursor solution. Moreover, it has been found that the increase of Cu(II) concentration in the solution facilitated the formation of binary phases such as Cu_6Sn_5 and Cu_5Zn_8.

There is still room to explore in greater depth the variables associated to this preparation route. Thus, the purpose of this work is to evaluate the influence of the electrodeposition time on the composition, structure, morphology, and final thickness of a metallic CZT precursor prepared by co-electrodeposition and followed by a reactive thermal sulfurization to obtain CZTS. In contrast to previous studies reported in the literature, our experimental conditions lead to high rates of deposition and films suitable to be incorporated in solar-cell prototypes, even electrodeposition times as short as 10–20 min.

2 Experimental

Fluorine-doped tin oxide glasses (FTO, from Pilkington TEC Glass, TEC 8, $\rho = 8\ \Omega\ sq^{-1}$) were used as substrates ($15 \times 10 \times 2$ and $20 \times 20 \times 2$ mm^3). The substrates were cleaned successively in detergent and isopropylic alcohol solution in an ultrasonic bath. A three-electrode cell, with a Pt mesh as counter electrode and a saturated calomel electrode (SCE) as reference electrode, were used. All the electrochemical potential values will be given against this reference, unless otherwise noted. Electrochemical measurements were carried out employing a PGZ 101 Voltalab® potentiostat/galvanostat. The electrolytic bath consisted of an acidic aqueous solution containing 0.03 mol L^{-1} $CuSO_4$, 0.1 mol L^{-1} $ZnSO_4$, and 0.01 mol L^{-1} $SnSO_4$. Also, 0.1 mol L^{-1} sodium citrate ($Na_3C_6H_5O_7$) was used as complexing agent with a final solution pH of 4. Prior to electrodeposition, the redox reactions of each of the various components of the electrolytic bath were analyzed by cyclic voltammetry. The voltammograms were recorded at 0.01 V s^{-1} and the potential was scanned first in the negative direction. Ternary precursor thin films (CZT) were electrodeposited in potentiostatic mode, applying a potential of −1.15 V. Deposition times between 10 and 40 min (CZT-10, CZT-20, CZT-30, and CZT-40) were explored to obtain different film thicknesses. The solution was purged with nitrogen prior to the electrodeposition to remove dissolved oxygen. After completing the electrodeposition, the samples were rinsed with distilled water and dried in air.

Electrodeposited CZT precursors were submitted to a reactive sulfurization annealing stage so as to obtain CZTS film. This thermal treatment was carried out in a three-temperature zone thermal reactor. First, the samples were placed in the cold zone of the tube (room temperature). Then the second zone was heated to 500 °C and in the third zone the sulfur powder (0.3 g) was allowed to reach 350 °C (melting starts at around

150 °C). At this point, the samples were moved to the second zone in order to start the sulfurization process, as the vaporized sulfur got in contact with the samples assisted by argon flux. After 1 h, the furnace was left to cool down naturally. These samples will be referred to as CZTS-10, CZTS-20, CZTS-30, and CZTS-40, where the number indicates the time in minutes used for the precursor (CZT) electrodeposition. Finally selected films were etched in a 0.5 mol L^{-1} KCN solution for 1 min in order to remove Cu_xS secondary phases and adjust the chemical composition of the film [27]. These samples were labeled with "E" at the end of the acronym to indicate the etching procedure (i.e., CZTS-10E and so on).

The crystalline structure of the as-deposited metallic precursors as well as of the sulfurized films was analyzed by X-ray diffraction using a PANalytical X'Pert PRO diffraction system employing Cu-Kα radiation at 40 kV and 40 mA. The samples were scanned between 15° and 80°, with a step size of 0.01°. The crystallographic data for each phase were taken from the literature [28].

Two scanning electron microscopes (JEOL JSM-6460LV and Carl Zeiss Supra 40 FESEM) were used to study the film morphology. The bulk elemental composition of CZTS films was analyzed by X-ray energy-dispersive spectroscopy (EDS) using an EDAX Genesis XM4—Sys 60 and Oxford Instruments, INCA processor. The composition of each film was calculated averaging three independent EDS measurements.

Raman spectroscopy measurements were performed using an Invia Reflex confocal Raman microprobe using a 50× objective. Excitation was provided with the 514 nm emission line of an Ar^+ laser. The laser power on the sample was less than 2 mW measured with a silicon photodiode (Coherent Inc.). For this condition, no thermal effects could be detected as a result of recording the Raman spectra. Raman maps were obtained scanning a square zone (80 × 80 µm) in the sample and recording a total of 25 spectra in the x and y directions. For both axes, the step between spectra was set in 20 µm.

A Shimadzu UV-3600 Plus spectrophotometer was employed to register transmission spectra in the wavelength range 700–1000 nm to calculate the band gap energy (E_{GAP}) by extrapolation. All the measurements were carried out at room temperature, using the FTO substrate as a reference.

The thickness of CZT and CZTS films was measured using a KLA TENCOR D-100 profilometer and compared with SEM cross-section images. Profilometry measurements were also used to calculate the roughness of the films using TalyProfile Gold software.

3 Results and discussion

3.1 Electrodeposition of CZT films

Figure 1 presents the voltammograms of FTO substrates in different electrolytes including only 0.1 mol L^{-1} sodium citrate (as a complexing agent, curve a) and solutions incorporating each individual ion: Cu^{2+} (curve b), Zn^{2+} (curve c), and Sn^{2+} (curve d) together with the electrochemical response of the FTO electrode in the precursor solution with all the ions present (curve e). Curve (a) shows that there is no electrochemical signal when using sodium citrate (NaCit) as electrolyte and FTO as substrate in this potential range. The cyclic voltammogram of copper ions (curve b) follows the reported complexing effect of citrate ions [29, 30] where the reduction of Cu^{2+} starts negative to −0.3 V with a broad cathodic peak around −0.6 V. The reduction of Zn^{2+} ions (curve c) starts at high negative potentials and seems to be overlapped with hydrogen evolution. In the reverse scan, an oxidation peak around −1.0 V confirms Zn deposition on FTO. Sn^{2+} ions start to reduce to metallic Sn around −0.8 V and in the anodic scan two peaks are observed at −0.7 and −0.55 V and attributed to the oxidation to Sn^{2+} and Sn^{4+} ions, respectively. From the preceding analysis, it is evident that the deposition of a precursor with a balanced composition is only possible at an electrodeposition potential negative to −1 V. In fact, electrodeposition potentials as negative as −1.63 V (vs. Ag/AgCl) have been employed to achieve a balance composition of the various elements [24]. Curve e shows the response of the system when all the ions are present. At potentials negative to −1.15 V, the current is dominated

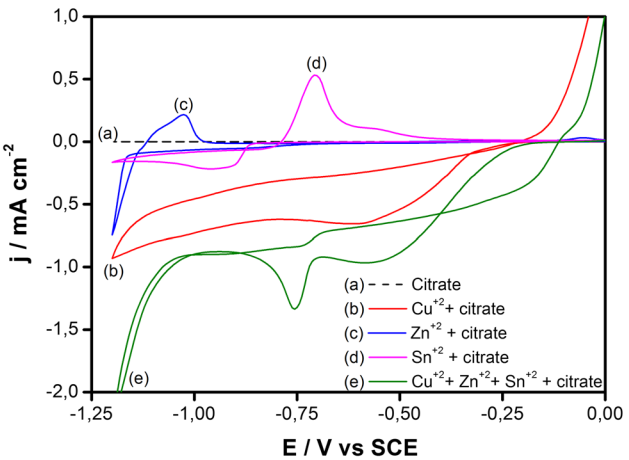

Fig. 1 Cyclic voltammograms of FTO in different electrolytes containing: (*a*) 0.1 mol L^{-1} NaCit, (*b*) 0.1 mol L^{-1} NaCit + 0.02 mol L^{-1} Cu^{2+}, (*c*) 0.1 mol L^{-1} NaCit + 0.1 mol L^{-1} Zn^{2+}, (*d*) 0.1 mol L^{-1} NaCit + 0.01 mol L^{-1} Sn^{2+} and, (*e*) CZT precursor electrolyte. *Scan rate* 0.01 V s^{-1}

by hydrogen evolution. To prevent delamination, the CZT electrodeposition was carried out at −1.15 V.

The chemical composition of CZT precursors was evaluated through EDS measurements. For films electrodeposited at different times on FTO substrates, the atomic composition for each element is shown in Table 1. Regardless of the deposition time, the films exhibit a high copper content, which is expected because its reduction potential is more favorable compared to those of tin and zinc. The zinc content appears to remain nearly constant at all deposition times, while the tin concentration in the film decreases with time at the expense of copper enrichment.

The chemical composition of CZTS films obtained by reactive sulfurization of the CZT precursors is presented in Table 2. In addition, changes after etching sulfurized films in KCN solutions are also included in this Table. After sulfurization, the samples show high contents of copper and sulfur which can be related with a material containing both CZTS and Cu_2S. Also, it can be seen that longer electrodeposition times produce precursors with higher copper contents, which after sulfurization could promote the formation of more Cu_2S. The amounts of zinc and tin in CZTS show a trend similar to that observed in the CZT precursors, where the tin content is higher than the Zn content only at the shortest electrodeposition time (10 min) and then decreases as the deposition time becomes longer. The effect of the KCN attack in the CZTS is quite significant in this case, where the copper concentration in the precursors and post-sulfurized CZT films is high. One minute immersion is enough to adjust the chemical composition of the films to values close to the stoichiometric formula of CZTS ($Cu_{25\%}Zn_{12.5\%}Sn_{12.5\%}S_{50\%}$). In turn, the CZTS films obtained from CZT-20, CZT-30, and CZT-40 present a Cu-poor and Zn-rich composition that matches the requirements for high efficiency CZTS photovoltaic devices [12].

The crystal structure of a CZT precursor electrodeposited during 40 min is analyzed in Fig. 2a. The diffractogram shows only characteristic peaks of the FTO substrate (SnO_2, PDF 77–0452) and a bimetallic compound identified as Cu_5Zn_8 (PDF 71-0397), also known as γ-brass, where Cu and Zn atoms are arranged in cubic unit cell. This intermetallic compound has been detected before by other authors in electrodeposited CZT films [23, 26]. No signals of tin, in its elemental state or alloyed with the others metals, are present in the diffractogram. As Sn was detected by EDS (see above), it is most likely present in amorphous state. No

Table 1 Chemical composition of electrodeposited CZT films

Sample	at.% Cu	at.% Zn	at.% Sn	Cu/Zn	Cu/Sn	Zn/Sn	Cu/(Zn + Sn)
CZT-10	60.94	18.54	20.52	3.29	2.97	0.90	1.56
CZT-20	62.89	18.78	18.33	3.35	3.43	1.02	1.69
CZT-30	64.41	20.68	14.90	3.11	4.32	1.39	1.81
CZT-40	67.78	20.64	11.58	3.28	5.86	1.78	2.10

Table 2 Chemical composition (at. %) of sulfurized CZT precursor films (CZTS) and KCN-etched CZTS thin films obtained by EDS

Sulfurized (500 °C 1 h)									
Sample	at.% Cu	at.% Zn	at.% Sn	at.% S	Cu/Zn	Cu/Sn	Zn/Sn	Cu/(Zn + Sn)	S/metal
CZTS-10	35.13	7.25	12.53	45.09	4.85	2.80	0.58	1.78	0.82
CZTS-20	38.33	12.43	9.64	39.60	3.08	3.97	1.29	1.74	0.66
CZTS-30	44.96	13.83	6.40	34.81	3.25	7.03	2.16	2.22	0.53
CZTS-40	45.18	13.57	8.27	32.98	3.33	5.46	1.64	2.07	0.49
Sulfurized (500 °C 1 h) + 1 min 0.5 mol L^{-1} KCN etching									
Etched sample	at.% Cu	at.% Zn	at.% Sn	at.% S	Cu/Zn	Cu/Sn	Zn/Sn	Cu/(Zn + Sn)	S/metal
CZTS-10	23.60	11.24	14.37	50.79	2.10	1.64	0.78	0.92	1.03
CZTS-20	22.52	14.43	12.46	50.59	1.56	1.81	1.16	0.84	1.02
CZTS-30	23.84	17.07	13.17	45.92	1.40	1.81	1.30	0.79	0.85
CZTS-40	22.06	16.75	13.75	47.44	1.32	1.60	1.22	0.72	0.90
Stoichiometric CZTS									
	at.% Cu	at.% Zn	at.% Sn	at.% S	Cu/Zn	Cu/Sn	Zn/Sn	Cu/(Zn + Sn)	S/metal
Cu_2ZnSnS_4	25	12.5	12.5	50	2	2	1	1	1

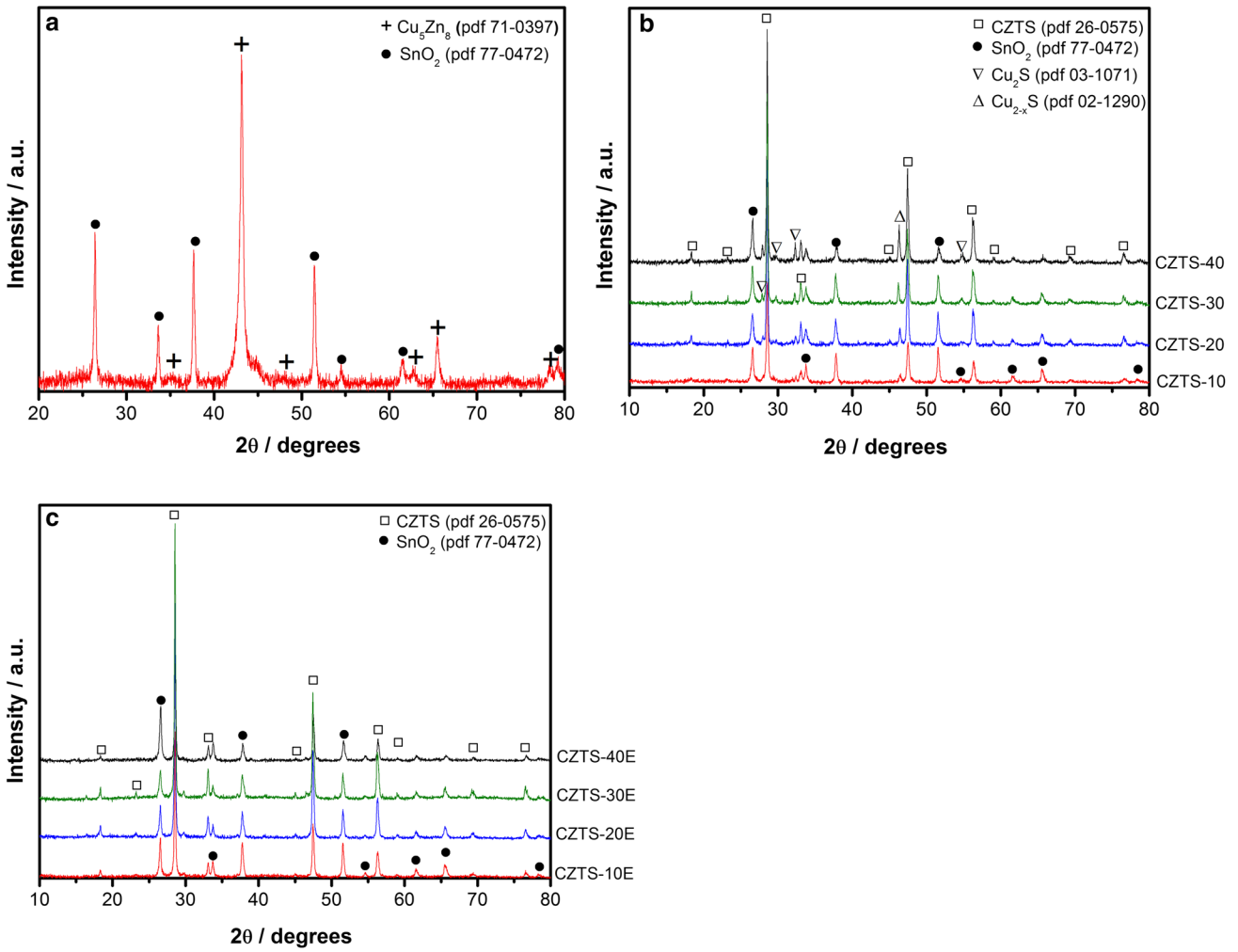

Fig. 2 XRD pattern of **a** CZT-40 film and **b** CZTS films **c** KCN-etched CZTS films

differences were found in the diffractogram when changing the electrodeposition time (not shown).

X-ray diffractograms of sulfurized CZT films prepared at different times (10–40 min) are presented in Fig. 2b. After sulfurization, CZT films transform into CZTS, and the XRD pattern satisfactorily matches the kesterite structure (PDF 26-0575, space group I-42m), which consists of a cubic close packing (ccp) array of anions, with cations occupying one-half of the tetrahedral voids. As it is observed in Fig. 2b, the peaks are intense, sharp, and narrow, as expected for a material with good crystalline degree. In addition, digenite or $Cu_{2-x}S$ (PDF 02-1292) and copper sulfide Cu_2S (PDF 03-1071) were also identified in the diffractogram. Copper sulfides are usually present in CZTS thin films as secondary phases [31–33]. Moreover, for CZTS films electrodeposited at longer times, the diffraction peaks assigned to these compounds are more intense indicating a higher proportion of these phases in the film. This confirms our previous observation related to the EDS results (Tables 1, 2) where longer electrodeposition times increase the copper content in the CZT precursor, which promotes $Cu_{2}^{-}{}_{x}S$ and Cu_2S formation after sulfurization. Chemical etching in KCN solutions is the standard procedure to remove copper sulfide compounds [32]. Diffraction patterns of treated films are presented in Fig. 2c. It can be seen that those peaks assigned to $Cu_{2-x}S$ and Cu_2S in the non-treated films are absent after etching.

Figure 3 presents Raman maps of sulfurized CZT precursor electrodeposited at different times, with and without KCN etching. Regardless of the deposition time, all spectra contain the main vibrational modes of the kesterite structure such as the A_1 principal mode found between 330 and 337 cm^{-1} and E(TO/LO) mode located between 280 and 290 cm^{-1} [34, 35]. As it was observed with XRD, aside from kesterite, copper sulfide is also present in sulfurized films as proved by the signal around 475 cm^{-1} characteristic of $Cu_2S/Cu_{2-x}S$ compounds [36]. Raman maps clearly show that this secondary phase is not as continuous as

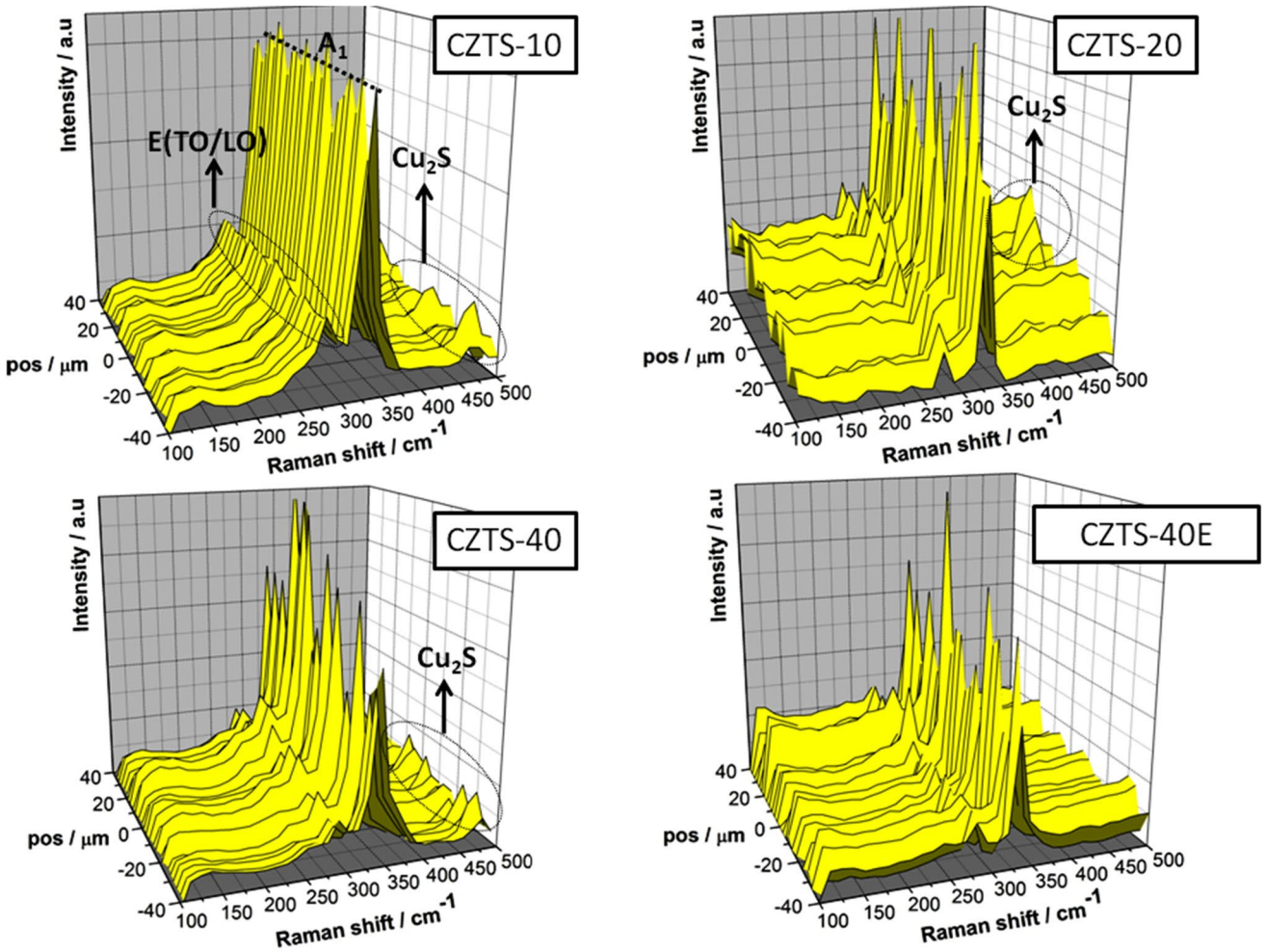

Fig. 3 Raman maps of selected CZT electrodeposited precursors at different times and sulfurized at 500 °C during 1 h. Also the effect of KCN etching is presented for a film electrodeposited at 40 min

kesterite is, appearing randomly along the surface. It can also be confirmed that films electrodeposited at longer times contain more $Cu_{2-x}S$ after sulfurization, as the characteristic signal is present in a larger number of spectra, in agreement with XRD and EDS results. Raman also confirms that undesired copper sulfide dissolves during KCN etching.

The changes in the morphology of the different films involved in this study can be followed by scanning electron microscopy (SEM). Images of the films synthesized using various electrodeposition times are presented in Fig. 4. The morphology of CZT precursors (CZT-10/CZT-40) is characteristic of a diffusion-controlled growth producing a so-called cauliflower-like structure frequently found in electrodeposited copper compounds like chalcopyrite or kesterite thin films [21, 37]. As the electrodeposition time increases, the cauliflower structure becomes bigger and branched, which indicates the growth of the nuclei formed at shorter times. At the shortest time (CZT10, Fig. 4), the agglomerates present nanometric sizes (100–300 nm) while at the longest time (CZT40, Fig. 4) the size of the agglomerates is in the micrometric scale. After sulfurization (CZTS-10/CZTS-40), the morphology of the film turns from the cauliflower structure to that of round-shape dispersed particles. This is a characteristic structure more related with a crystalline material, as it was confirmed previously with XRD and Raman spectroscopy. After KCN etching, besides the change in the chemical composition, the morphology of the film is altered and seems to turn into a more refined structure. This effect is more pronounced for films deposited at longer times where diffusion-controlled growth becomes dominant.

Cross-section pictures corresponding to CZT, CZTS, and CZTS-E films are shown in Fig. 5. For the as-deposited film elongated "cauliflower," branches arise from the top of the FTO substrate mainly at electrodeposition times higher than 20 min. It seems to be an open structure with some degree of porosity. Gougaud et al. [38] have reported

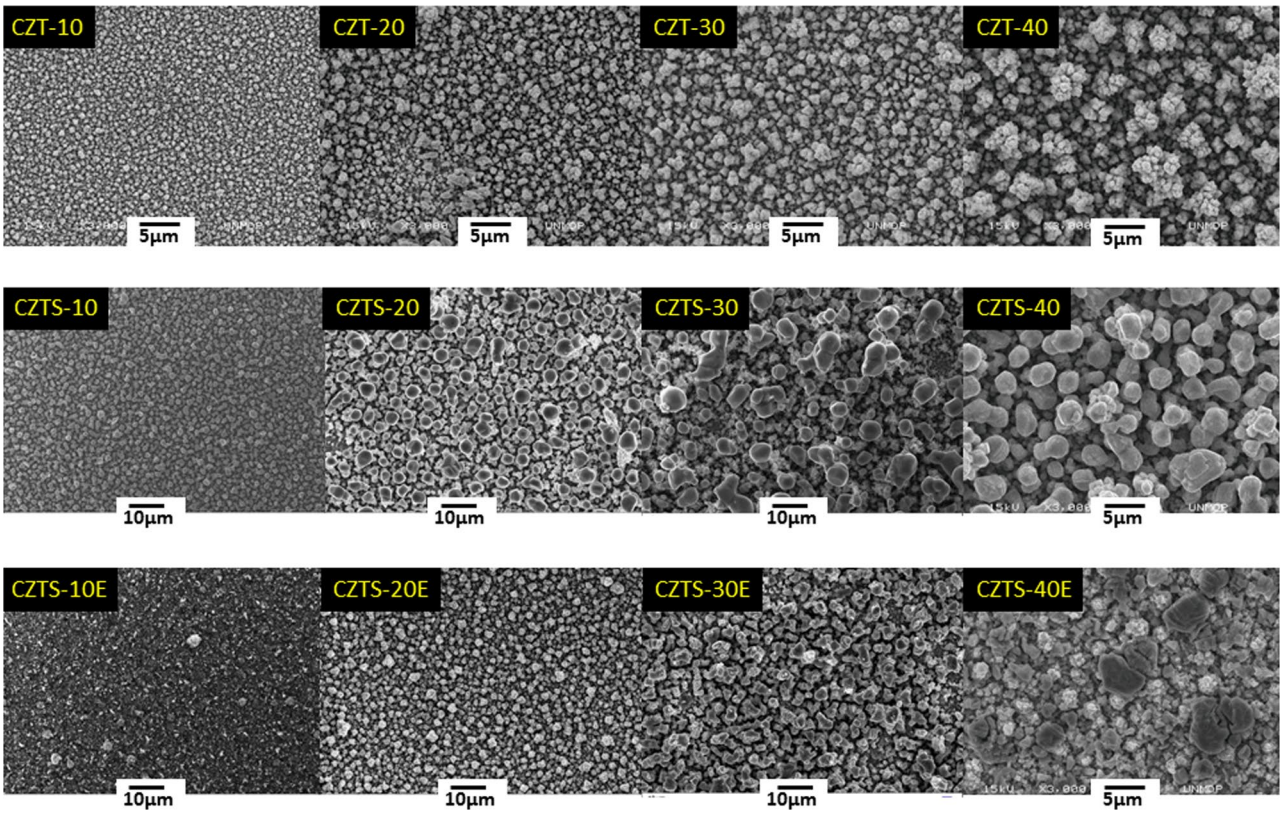

Fig. 4 Top view SEM pictures of electrodeposited CZT precursors, CZTS films and KCN-etched CZTS films

this kind of dendritic structure with an irregular thickness which is normally found in electrodeposited copper and zinc from a sulfate bath and it is produced by a diffusion-controlled process. After sulfurization and transformation of CZT into CZTS, all the films become thicker. This can be taken as an evidence of thermal expansion of the material during annealing. Scragg et al. [39] have reported a similar behavior after sulfurization of electrodeposited elemental staked layers with a thermal expansion factor of 2.7. Jeon et al. [40] have reported a significant vertical expansion due to Se incorporation during selenization of CZT metallic precursors. In our films, an expansion factor between 2 and 3 has been found depending on the precursor electrodeposition time. In addition, a bi-layered structure is observed, with a compact and more refined structure near the FTO substrate and a second layer formed by bigger particles deposited on the top, especially at higher deposition times. In order to provide more evidence of this phenomenon, Fig. 6 presents cross-section SEM pictures of a CZTS film obtained via sulfurization of a CZT-40 precursor. This kind of bi-layered structure was also previously reported in co-electrodeposited kesterite films [41, 42]. Regarding this, it is likely that thicker precursor films (mainly CZT-30 and CZT-40) may need longer sulfurization times to reach a more uniform and compact structure as that observed starting out with thinner precursors (CZTS-20 and CZTS-10). This implies that sulfurization times must be adjusted to the precursor thickness after electrodeposition to optimize the structure and morphology of the resulting CZTS film. In our samples, 60 min of sulfurization are enough to consolidate and produce a compact CZTS structure for a precursor film electrodeposited during 10 min, which after KCN etching presents an average thickness close to 2.5 μm (CZTS-10E).

Also, the bi-layered structure could be related to the fact that longer electrodeposition times produce more Cu_xS secondary phase co-existing with the CZTS. Furthermore, due to the thermal expansion of the precursor after sulfurization, electrodeposition times of 30 and 40 min produce films with thicknesses that surpass the optimal thickness for an absorber material in a thin film solar cell that is between 2 and 3 μm [43]. For additional comparison, a typical profilometry measurement of each film is inserted in Fig. 5. Table 3 summarizes average values for film thicknesses registered with both methods. At shorter and intermediate electrodeposition times, both techniques give comparative thickness values, while at the longest time (40 min) the measurements are less accurate, especially for the values extracted by SEM images. The thickness registered by profilometry seems

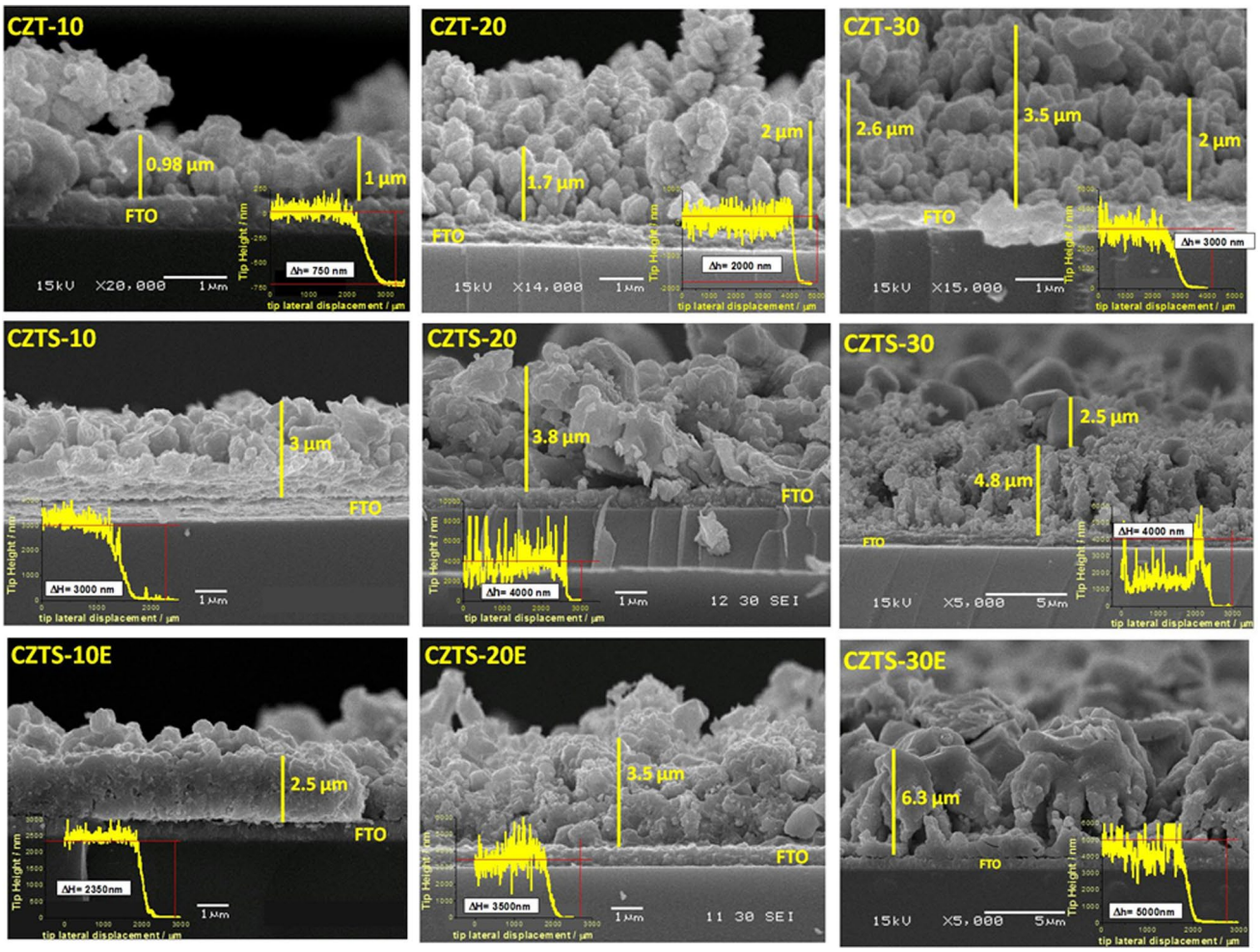

Fig. 5 Cross-section SEM pictures of electrodeposited CZT precursors, CZTS films, and KCN-etched CZTS films. A profilometry measurement of each film is inserted for sake of comparison

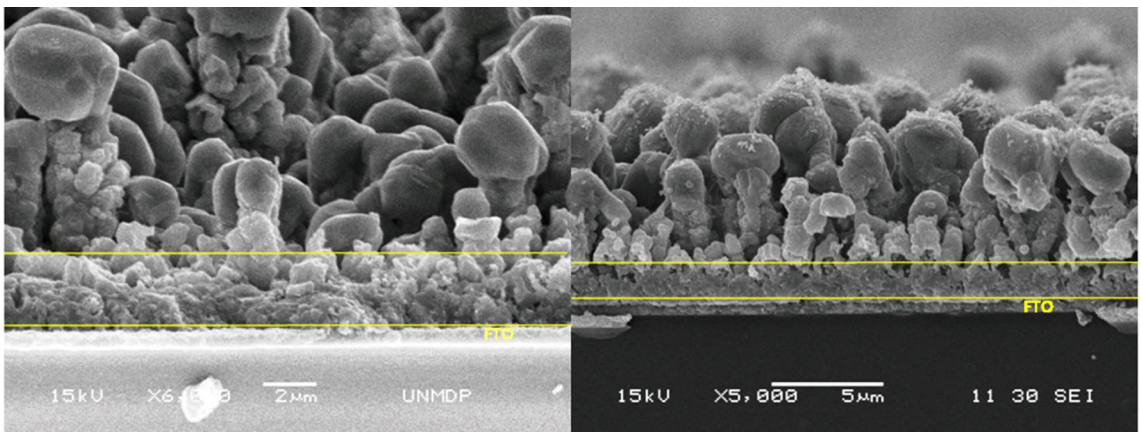

Fig. 6 Cross-section SEM pictures of a CZTS-40 film showing the bi-layered structure

Table 3 Film thicknesses of electrodeposited CZT, CZTS, and KCN-etched CZTS films estimated using profilometry and cross-section SEM images

Sample	Profilometer/μm	SEM/μm	Roughness (Ra)/μm
Electrodeposited CZT films			
CZT-10	0.68 ± 0.11	0.98 ± 0.07	0.031 ± 0.004
CZT-20	1.65 ± 0.21	1.93 ± 0.38	0.14 ± 0.04
CZT-30	1.95 ± 0.49	1.55 ± 0.21	0.15 ± 0.04
CZT-40	2.45 ± 0.35	6.49 ± 1.56	0.18 ± 0.10
Sulfurized CZT films			
CZTS-10	2.65 ± 0.21	3.03 ± 0.16	0.17 ± 0.04
CZTS-20	3.75 ± 0.35	3.61 ± 0.36	0.38 ± 0.04
CZTS-30	4.00 ± 0.4	5.93 ± 0.55	0.60 ± 0.08
CZTS-40	7.35 ± 0.49	7.51 ± 0.90	0.92 ± 0.11
KCN-etched CZTS films			
CZTS-10E	2.33 ± 0.04	2.36 ± 0.18	0.07 ± 0.01
CZTS-20E	3.38 ± 0.18	3.34 ± 0.39	0.29 ± 0.11
CZTS-30E	4.33 ± 0.29	7.51 ± 0.30	0.39 ± 0.05
CZTS-40E	x	x	x

The roughness of each film expressed via the arithmetic mean roughness profile factor (Ra) is also included

to be an average value of those extracted using cross-section SEM images. However, the films show some degree of roughness. Arithmetic mean roughness profile factor (Ra) values are also presented in Table 3. Precursor films present lower roughness than sulfurized ones and after etching the roughness reduces again in agreement with the analysis of SEM top view images of etched CZTS films (Fig. 4). Moreover, film roughness seems to increase as the thickness of the films grows, indicating that longer electrodeposition times produce less homogenous deposits.

On the basis of previously published works, we expected to obtain CZT precursors with thicknesses between 1 and 2 μ using electroplating times between 10 and 40 min. For instance, in the work of Gurav et al. [21], the experimental conditions to prepare CZTS thin films are very similar to those reported in this work with the difference that the substrate is Mo sputtered glass instead of FTO. Also, the authors used H_2S during the sulfurization stage and reported thicknesses lower than 1 μ of CZTS films electrodeposited during 40 min and sulfurized at 580 °C for 1 h. Our CZT films surpass the micron barrier with only 10 min of electrodeposition and agree better with the results reported by Lee et al. [22], even if still thicker at equal electrodeposition times. Despite this contrast, our results suggest a higher rate of deposition and formation of the precursor, which from and industrial point of view is more attractive. 10 minutes are enough to produce a precursor with a thickness close to the micron that after the thermal treatment reaches a thickness suitable for an absorber in thin film solar cell.

Figure 7a presents optical measurements centered in the near-infrared region and the corresponding bandgap energy E_{GAP} calculation (Fig. 7b) for sulfurized CZT precursors, after KCN etching. In fact, all the transmittance spectra show a sharp fall for wavelengths below 850 nm, where an absorption edge corresponding to direct band-to-band transition is present. For all the films, the transmittance of radiation varies between 20 and 40%. This can be expected, given that the thickness of these films is relatively high, as discussed above. The values of transmittance in this transparency region are originated in light dispersion which may

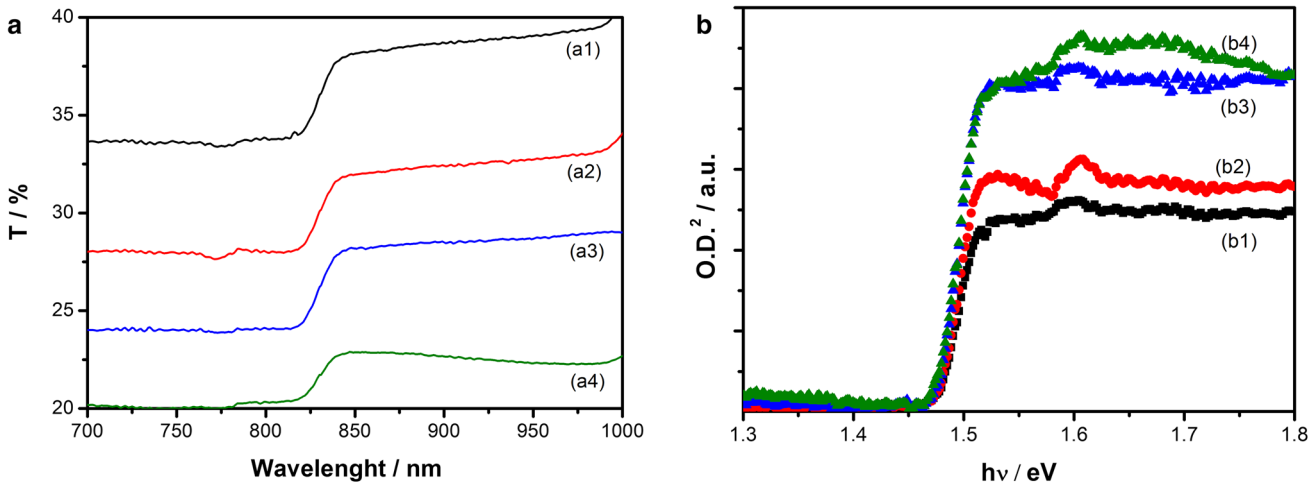

Fig. 7 **a** Transmittance spectra in the IR region of sulfurized CZT precursors: (a_1) CZTS-10E, (a_2) CZTS-20E, (a_3) CZTS-30E; and (a_4) CZTS-40E. **b** Energy gap (E_{GAP}) estimation according to the procedure described in the text. (b_1) CZTS-10E, (b_2) CZTS-20E, (b_3) CZTS-30E, and (b_4) CZTS-40E

depend on sample morphology. From the transmittance (T), the experimental optical density (OD), also called absorbance, can be calculated as $OD = -\log_{10} T$ [44]. Based on the allowed direct interband transition, the energy gap (E_{GAP}) value can be determined from a plot of the optical density $(OD)^2$ versus photon energy ($h\nu$), which shows a linear region. The corresponding E_{GAP} can be obtained by extrapolating a linear fitting from the $(OD)^2$ versus $h\nu$ plot, finding the energy value where this linear fitting intersects the horizontal photon energy axis [44, 45]. Plots for the different films are included in Fig. 7b with their corresponding extrapolation to estimate of the band gap energy, resulting in $E_{GAP} = 1.47$ eV. E_{GAP} values are in agreement with those reported in the literature for the pure sulfur kesterite Cu_2ZnSnS_4 that presents an energy gap close to 1.5 eV [21, 23]. The evaluation of different films shows that electrodeposition times do not seem to affect the energy gap.

4 Conclusions

CZTS films were successfully deposited on FTO from electrodeposited CZT precursors and further sulfurized by annealing in S-rich atmosphere. The electrodeposition time significantly affects the chemical composition of the precursor, with especial influence in the Cu and Sn content. CZT precursors present a cauliflower-like morphology, especially at long deposition times, which is typical of an electrodeposition mechanism controlled by mass transfer. However after sulfurization, Raman spectroscopy, XRD, and EDS measurements confirm the formation of crystalline CZTS. Also, Cu_xS compounds co-exist dispersed in the film. Raman and XRD analysis reveal that the amount of secondary phases increases with longer electrodeposition times. After sulfurization the film thickness increases between 2 and 3 times indicating a thermal expansion of the CZT precursor. Moreover, CZTS films obtained from precursor electrodeposited at longer times (30–40 min) present a bi-layered structure pointing out that the sulfurization time was only enough to consolidate films obtained at shortest electrodeposition times (thinner CZT precursors). Further from the well-known effect of Cu_xS removal, a short treatment in KCN solution seems to produce a certain degree of particle refining and surface smoothing. A direct energy gap of 1.47 eV was estimated for CZTS films using transmittance spectra in the infrared region. Etched CZTS films obtained from 10 to 20 min electrodeposited precursors end up having a suitable composition, structure, and thickness for their potential incorporation in a PV device.

Acknowledgements This study was supported by the *Consejo Nacional de Investigaciones Científicas y Técnicas* (CONICET Argentina) and the *Agencia Nacional de Investigación e Innovación* (ANNI) under the bilateral cooperative Project CONICET/ANII Nº R36535. Financial support from *Universidad Nacional de Mar del Plata* (UNMdP) and *Universidad de la República*, in Montevideo, Uruguay is also highly acknowledged. R. E. M. also acknowledges CSIC, PEDECIBA – Física, and ANII (Projects MOV_CO_2013_1_100005 and FSE_1_2014_1_102184), Uruguay.

References

1. Ito K, Nakazawa T (1988) Electrical and optical properties of stannite-type quaternary semiconductor thin films. Jpn J Appl Phys 27(11):2094–2097
2. Siebentritt S, Schorr S (2012) Kesterites—a challenging material for solar cells. Prog Photovolt Res Appl 20(5):512–519. doi:10.1002/pip.2156
3. Kim S, Kim KM, Tampo H, Shibata H, Matsubara K, Niki S (2016) Ge-incorporated $Cu_2ZnSnSe_4$ thin-film solar cells with efficiency greater than 10%. Sol Energy Mater Sol Cells 144:488–492. doi:10.1016/j.solmat.2015.09.039
4. Hages CJ, Koeper MJ, Agrawal R (2016) Optoelectronic and material properties of nanocrystal-based CZTSe absorbers with Ag-alloying. Sol Energy Mater Sol Cells 145:342–348. doi:10.1016/j.solmat.2015.10.039
5. Fu X, Ji Z, Li C, Zhou Z (2016) Electrochemical method for synthesis of Cu_2ZnSnS_4 Nanorod/TiO_2 nanotube arrays hybrid structure with enhanced photoelectrochemical properties. J Alloys Compd 688:1013–1018. doi:10.1016/j.jallcom.2016.07.127
6. Chaudhari S, Palli S, Kannan PK, Dey SR (2016) Pulsed electrodeposition of Cu_2ZnSnS_4 absorber layer precursor for photovoltaic application. Thin Solid Films 600:169–174. doi:10.1016/j.tsf.2016.01.021
7. Tian Q, Cui Y, Wang G, Pan D (2015) A robust and low-cost strategy to prepare Cu_2ZnSnS_4 precursor solution and its application in $Cu_2ZnSn(S,Se)_4$ solar cells. RSC Adv 5(6):4184–4190. doi:10.1039/c4ra12090f
8. Gamburg YD, Zangari G (2011) Theory and practice of metal electrodeposition. Springer, New York. doi:10.1007/978-1-4419-9669-5
9. Colombara D, Crossay A, Vauche L, Jaime S, Arasimowicz M, Grand PP, Dale PJ (2015) Electrodeposition of kesterite thin films for photovoltaic applications: quo vadis? Phys Status Solidi A 212(1):88–102. doi:10.1002/pssa.201431364
10. Mitzi DB, Gunawan O, Todorov TK, Wang K, Guha S (2011) The path towards a high-performance solution-processed kesterite solar cell. Sol Energy Mater Sol Cells 95(6):1421–1436
11. Scragg JJ, Berg DM, Dale PJ (2010) A 3.2% efficient Kesterite device from electrodeposited stacked elemental layers. J Electroanal Chem 646(1–2):52–59
12. Vauche L, Risch L, Sánchez Y, Dimitrievska M, Pasquinelli M, Goislard de Monsabert T, Grand PP, Jaime-Ferrer S, Saucedo E (2015) 8.2% Pure selenide kesterite thin-film solar cells from large-area electrodeposited precursors. Prog Photovolt Res Appl. doi:10.1002/pip.2643
13. Jiang F, Ikeda S, Harada T, Matsumura M (2014) Pure Sulfide Cu_2ZnSnS_4 thin film solar cells fabricated by preheating an electrodeposited metallic stack. Adv Energy Mater. doi:10.1002/aenm.201301381
14. Pawar SM, Pawar BS, Moholkar AV, Choi DS, Yun JH, Moon JH, Kolekar SS, Kim JH (2010) Single step electrosynthesis of Cu_2ZnSnS_4 (CZTS) thin films for solar cell application. Electrochim Acta 55(12):4057–4061
15. Cui Y, Zuo S, Jiang J, Yuan S, Chu J (2011) Synthesis and characterization of co-electroplated Cu_2ZnSnS_4 thin films as

potential photovoltaic material. Sol Energy Mater Sol Cells 95(8):2136–2140
16. Ge J, Jiang J, Yang P, Peng C, Huang Z, Zuo S, Yang L, Chu J (2014) A 5.5% efficient co-electrodeposited ZnO/CdS/Cu_2ZnSnS_4/Mo thin film solar cell. Sol Energy Mater Sol Cells 125:20–26
17. Valdes M, Modibedi M, Mathe M, Hillie T, Vazquez M (2014) Electrodeposited Cu_2ZnSnS_4 thin films. Electrochim Acta 128:393–399
18. Ennaoui A, Lux-Steiner M, Weber A, Abou-Ras D, Kötschau I, Schock HW, Schurr R, Hölzing A, Jost S, Hock R, Voß T, Schulze J, Kirbs A (2009) Cu_2ZnSnS_4 thin film solar cells from electroplated precursors: novel low-cost perspective. Thin Solid Films 517(7):2511–2514
19. Araki H, Kubo Y, Jimbo K, Maw WS, Katagiri H, Yamazaki M, Oishi K, Takeuchi A (2009) Preparation of Cu_2ZnSnS_4 thin films by sulfurization of co-electroplated Cu–Zn–Sn precursors. Phys Status Solidi (A) 6(5):1266–1268
20. Wang Y, Ma J, Liu P, Chen Y, Li R, Gu J, Lu J, Yang SE, Gao X (2012) Cu_2ZnSnS_4 films deposited by a co-electrodeposition-annealing route. Mater Lett 77:13–16
21. Gurav KV, Pawar SM, Shin SW, Suryawanshi MP, Agawane GL, Patil PS, Moon JH, Yun JH, Kim JH (2013) Electrosynthesis of CZTS films by sulfurization of CZT precursor: effect of soft annealing treatment. Appl Surf Sci 283:74–80
22. Lee KD, Seo SW, Lee DK, Kim H, Jeong JH, Ko MJ, Kim B, Kim DH, Kim JY (2013) Preparation of Cu_2ZnSnS_4 thin films via electrochemical deposition and rapid thermal annealing. Thin Solid Films 546:294–298
23. Li Y, Yuan T, Jiang L, Su Z, Liu F (2014) Growth and characterization of Cu_2ZnSnS_4 photovoltaic thin films by electrodeposition and sulfurization. J Alloys Compd 610:331–336. doi:10.1016/j.jallcom.2014.05.014
24. He X, Shen H, Wang W, Pi J, Hao Y, Shi X (2013) Synthesis of Cu_2ZnSnS_4 films from co-electrodeposited Cu–Zn–Sn precursors and their microstructural and optical properties. Appl Surf Sci 282:765–769. doi:10.1016/j.apsusc.2013.06.050
25. Cheng K, Meng J, Wang X, Huang Y, Liu J, Xue M, Du Z (2015) Low-cost Cu_2ZnSnS_4 thin films prepared from single step electrodeposited Cu/Zn/Sn alloy precursor films. Mater Chem Phys 163:24–29. doi:10.1016/j.matchemphys.2015.06.026
26. Hreid T, Li J, Zhang Y, Spratt HJ, Wang H, Will G (2015) Effects of metal ion concentration on electrodeposited CuZnSn film and its application in kesterite Cu_2ZnSnS_4 solar cells. RSC Adv 5(80):65114–65122. doi:10.1039/c5ra09966h
27. Buffière M, Brammertz G, Sahayaraj S, Batuk M, Khelifi S, Mangin D, El Mel AA, Arzel L, Hadermann J, Meuris M, Poortmans J (2015) KCN chemical etch for interface engineering in $Cu_2ZnSnSe_4$ solar cells. ACS Appl Mater Interfaces 7(27):14690–14698. doi:10.1021/acsami.5b02122
28. International Centre for Diffraction Data (ICCD) (1998). Powder diffraction file database. EEUU, Newtown. Square
29. Ren P, Dai N, Deng HY, Zhang JX (2015) Growth kinetics and microstructures of Cu nanofilms on Mo substrate by electrodeposition. J Electrochem Soc 162(1):D9–D14. doi:10.1149/2.0221501jes
30. Shin S, Park C, Kim C, Kim Y, Park S, Lee J-H (2016) Cyclic voltammetry studies of copper, tin and zinc electrodeposition in a citrate complex system for CZTS solar cell application. Curr Appl Phys 16 (2):207–210. doi:10.1016/j.cap.2015.11.017
31. Just J, Ltzenkirchen-Hecht D, Frahm R, Schorr S, Unold T (2011) Determination of secondary phases in kesterite Cu 2ZnSnS 4 thin films by X-ray absorption near edge structure analysis. Appl Phys Lett 99:26
32. Buffière M, Brammertz G, Sahayaraj S, Batuk M, Khelifi S, Mangin D, El Mel AA, Arzel L, Hadermann J, Meuris M, Poortmans J (2015) KCN chemical etch for interface engineering in Cu_2ZnSnS_4 solar cells. ACS Appl Mater Interfaces 7(27):14690–14698. doi:10.1021/acsami.5b02122
33. Kim GY, Jo W, Lee KD, Choi HS, Kim JY, Shin HY, Nguyen TTT, Yoon S, Joo BS, Gu M, Han M (2015) Optical and surface probe investigation of secondary phases in Cu_2ZnSnS_4 films grown by electrochemical deposition. Sol Energy Mater Sol Cells 139:10–18. doi:10.1016/j.solmat.2015.03.003
34. Gürel T, Sevik C, ÇağIn T (2011) Characterization of vibrational and mechanical properties of quaternary compounds Cu_2ZnSnS_4 and $Cu_2ZnSnSe_4$ in kesterite and stannite structures. Phys Rev B 84 (20):205201
35. Fontané X, Izquierdo-Roca V, Saucedo E, Schorr S, Yukhymchuk VO, Valakh MY, Pérez-Rodríguez A, Morante JR (2012) Vibrational properties of stannite and kesterite type compounds: Raman scattering analysis of Cu 2(Fe,Zn)SnS 4. J Alloys Compd 539:190–194
36. Fernandes PA, Salomé PMP, da Cunha AF (2009) Growth and Raman scattering characterization of Cu_2ZnSnS_4 thin films. Thin Solid Films 517(7):2519–2523
37. Whang T-J, Hsieh M-T, Kao Y-C (2010) Studies of single-step electrodeposition of $CuInSe_2$ thin films with sodium citrate as a complexing agent. Appl Surf Sci 257(5):1457–1462. doi:10.1016/j.apsusc.2010.08.072
38. Gougaud C, Rai D, Delbos S, Chassaing E, Lincot D (2013) Electrochemical studies of one-step electrodeposition of Cu-Sn-Zn layers from aqueous electrolytes for photovoltaic applications. J Electrochem Soc 160:D485–D494. doi:10.1149/2.105310jes
39. Scragg JJ (2011) Copper zinc tin sulfide thin films for photovoltaics. Springer, Berlin. doi:10.1007/978-3-642-22919-0
40. Jeon J-O, Lee KD, Seul Oh, Seo S-W, Lee D-K, Kim H, Jeong J-H, Ko MJ, Kim B, Son HJ, Kim JY (2014) Highly efficient copper-zinc-tin-selenide (CZTSe) solar cells by electrodeposition. ChemSusChem 7(4):1073–1077. doi:10.1002/cssc.201301347
41. Tao J, Zhang K, Zhang C, Chen L, Cao H, Liu J, Jiang J, Sun L, Yang P, Chu J (2015) A sputtered CdS buffer layer for co-electrodeposited Cu_2ZnSnS_4 solar cells with 6.6% efficiency. Chem Commun 51(51):10337–10340. doi:10.1039/c5cc01170a
42. Vauche L, Dubois J, Laparre A, Pasquinelli M, Bodnar S, Grand PP, Jaime S (2015) Rapid thermal processing annealing challenges for large scale Cu_2ZnSnS_4 thin films. Phys Status Solidi A 212(1):103–108. doi:10.1002/pssa.201431387
43. Luque A, Hegedus S (2003) Handbook of photovoltaic science and engineering. Wiley, West Sussex.
44. Fox M (2001) Optical properties of solids. Oxford University Press, New York.
45. Tanaka T, Nagatomo T, Kawasaki D, Nishio M, Guo Q, Wakahara A, Yoshida A, Ogawa H (2005) Preparation of Cu_2ZnSnS_4 thin films by hybrid sputtering. J Phys Chem Solids 66(11):1978–1981